Power loss mechanisms in n-type modulation-doped AlGaAs/GaAsBi quantum well heterostructures

O. Donmez[1,*], M. Aydın[1], Ş. Ardalı[2], S. Yıldırım[1], E. Tıraş[2], A. Erol[1], J. Puustinen[3], J. Hilska[3], M. Guina[3]

[1]Department of Physics, Faculty of Science, Istanbul University, Vezneciler, 34134, Istanbul, Turkey

[2]Faculty of Science, Department of Physics, Eskişehir Technical University, Tepebaşı, Eskişehir 26470, Turkey

[3]Optoelectronics Research Centre, Physics Unit, Tampere University, Korkeakoulunkatu 3, 33720 Tampere, Finland

*E-mail: omerdonmez@istanbul.edu.tr

Abstract: We report on the power loss mechanisms of hot electrons in as-grown and annealed n-type modulation-doped $Al_{0.15}Ga_{0.85}As/GaAs_{1-x}Bi_x$ (x = 0 and 0.04) quantum well (QW) structures considering acoustic phonon interactions *via* the deformation potential (non-polar) and piezoelectric (polar) scatterings. The two-dimensional (2D) electron gas is heated by applying various electric fields under a steady-state magnetic field, and the effect of the applied electric field on the Shubnikov de Haas (SdH) oscillations is analyzed to investigate the power loss mechanism. The temperature of hot electrons (T_e) has been obtained by comparing the lattice temperature and applied electric field dependencies of the SdH oscillation amplitude. The hot electron temperature is almost the same for both Bi-free and Bi-containing samples except for the sample annealed at higher temperature (700°C) than the growth temperature of GaAsBi. The electron temperature dependence of power loss is analyzed using current theoretical analytic models derived for 2D semiconductors. We find that energy relaxation occurs in the intermediate temperature regime, including mixing of piezoelectric and deformation potential scattering. The power loss of hot electrons is found to be proportional to $(T_e^{\gamma} - T_L^{\gamma})$ with γ in the range from 2.4 to 4.2, which indicates that the hot electron relaxation is due to acoustic phonon scatterings *via* unscreened deformation potential and piezoelectric scattering. It is found that deformation potential scattering is dominant over piezoelectric scattering in the Bi-free sample, while the incorporation of Bi into the GaAs lattice makes these processes comparable. After thermal annealing at lower than growth temperature (350°C), the scattering mechanism switches from deformation potential to piezoelectric scattering. After thermal annealing at higher than growth temperature (700°C), the theoretical model does not fit to the experimental results due to degradation of the sample.

Keywords: hot electron in GaAsBi; power loss; acoustic phonon scattering, n-type modulation doped GaAsBi quantum well, energy relaxation

Introduction

Shrinking of semiconductor devices to the micro/nanoscale results in the generation of hot carriers under the application of small voltages due to strong electric fields. The physics of hot carriers is based on non-linear effects related to the energy and momentum exchange between hot carriers and phonons, and/or between impurities and photons. Therefore, the study of energy and momentum relaxation mechanisms of hot carriers is essential for understanding the operation of novel semiconductor devices in a non-linear transport regime under high electric fields.

$GaAs_{1-x}Bi_x$ is a novel highly mismatched alloy which has attracted great attention due to its promising properties, such as higher flexibility in tuning the band gap [1–4], and allows the fabrication of novel semiconductor optoelectronic devices for the near- and mid-IR regions of the electromagnetic spectrum[5,6], as well as spintronic devices [7,8]. Semiconductor devices are essentially based on low dimensional structures, such as quantum wells (QW). However, in order to design novel GaAsBi QW-based low dimensional devices, quantum transport mechanisms under large electric fields have to be understood. As the device sizes become comparable to the de Broglie wavelength of the charge carriers, even a small voltage creates very high electric fields and leads to the generation of hot carriers. Therefore, the physics of hot carries and their power loss mechanisms have to be well understood.

Most of the published papers on the GaAsBi alloy have focused on the fundamental properties of the material, such as the Bi-dependence of band structures, optical and structural properties *etc*. Even though GaAsBi-based semiconductor lasers have been fabricated, the influence of Bi on the electrical transport properties of the material have been investigated in a very limited number of papers. So far, the composition dependence of the electron and hole mobility and the temperature dependence of carrier mobility have been reported [9–12]. Furthermore, Bi-related electron and hole effective masses have been reported for n- type GaAsBi epilayer structures [13]. In a recent study [14], we have reported that for n-type modulation doped as-grown and annealed GaAsBi/AlGaAs QW structures, there is no significant direct effect of Bi on the electron effective mass, however there is an indirect effect, in which Bi can provoke changes in the 2D electron density. In addition, our recent results have revealed that both the quantum mobility and quantum scattering time of electrons decrease as an effect of possible Bi-related

scattering mechanisms such as interface, alloy and impurity scatterings in n-type modulation doped GaAsBi/AlGaAs QW structures. Apart from these very limited studies on electron transport properties of GaAsBi-based QW structures, to the best of our knowledge, the power loss mechanisms of hot electron in GaAsBi QW structures are yet to be published.

In the high electric field transport regime, the fundamentals of electronic and optoelectronic devices are governed by electron-phonon scattering, therefore determination of the energy relaxation mechanisms and electron temperature under high electric field gives useful information for the design of devices. Comparison of experimental techniques for the investigation of energy relaxation of electrons can be found in reference [15]. In heavily modulation doped QW structures, the power loss mechanisms of hot carriers *via* electron-phonon scatterings can be determined by analyzing SdH oscillations under electric field heating [15–18]. The SdH oscillation method assumes that, since the density of optical phonons is negligible below ~40 K, the energy relaxation of hot electrons can be achieved by acoustic phonon scattering (inelastic scattering). It is also assumed that the contribution of elastic scattering mechanisms such as the remote ionized impurity scattering, alloy scattering and interface roughness can be ignored at low temperatures [16,17,19].

In this paper, we present an analysis of the power loss mechanisms in the scheme of acoustic phonon-assisted cooling of the 2D hot electron gas in n-type modulation doped as-grown and annealed $Al_{0.15}Ga_{0.85}As/GaAs_{1-x}Bi_x$ (x = 0, and 0.04) QW structures. The modulation doped samples are highly degenerate, therefore the SdH oscillations in magnetoresistance as a function of an applied electric field are employed to determine the temperature of hot electrons and the corresponding power loss mechanisms.

Experimental

An n-type modulation doped $Al_{0.15}Ga_{0.85}As/GaAs_{0.96}Bi_{0.04}$ QW structure was grown on semi-insulating GaAs using molecular beam epitaxy. In addition, a reference sample without Bi ($Al_{0.15}Ga_{0.85}As/GaAs$) was grown. The QW layer in the GaAsBi sample was grown at 370°C, while the GaAs QW for the reference sample was grown at a typical GaAs growth temperature of 580°C. The sample structures are listed in Table I. Growth details can be found in Refs. [14,20]. The samples were processed in the form of

the Hall bar bridge using standard photolithography techniques, and Ohmic contacts were obtained by alloying Au/Ge/Ni.

In order to determine the effect of thermal annealing on the power loss mechanisms of the 2D electron gas, post-growth rapid thermal annealing was applied under N_2 gas to the Bi containing sample at 700°C for 60s and at 350°C for 180s. The samples were capped with a GaAs wafer during thermal annealing. The sample codes used in this report are presented in Table II. It is worth noting that we conducted photoluminescence (PL) measurements for the samples annealed at temperatures above (550°C, 600°C, 650°C and 700°C for 60 s) and below (350°C for 60 s and 180 s) the growth temperature of the GaAsBi QW layer. We observed that annealing at temperatures above the growth temperature decreased the PL intensity. The highest PL intensity is observed for the sample annealed at 350°C for 180 s. The optical characterization of the as-grown and annealed samples is out of the scope of this paper; therefore, we do not further discuss PL results here. Since we have observed an opposite effect from annealing at higher and lower temperatures than the growth temperature of GaAsBi layer, we have focused magnetoresistance measurements on the samples annealed at 700°C (TNBi04A) for 60s and at 350°C for 180s (TNBi04B). The power loss mechanisms of the 2D electron gas were studied using magnetoresistance measurements. An Oxford-Heliox-VL ^{3}He cryostat equipped with a 20 T superconducting magnet was employed to apply a perpendicular steady magnetic field to the plane of the 2D electron gas at 4.2 K, and a uniform and steady (dc) current between $50\,\mu A$ and $2300\,\mu A$ was applied in-plain to the 2D electron gas. The experiments were carried out as a function of electric field at 4.2 K.

Table I : Structure of the experimental samples.

Material	**Thickness (nm)**	**Dopant atom /density**	T_{growth}
GaAs (cap)	5	Si- $5 \times 10^{17}\mathrm{cm}^{-3}$	580°C
$Al_{0.15}Ga_{0.85}As$ **(**barrier)	10	Si -1$\times 10^{18}\mathrm{cm}^{-3}$	
$Al_{0.15}Ga_{0.85}As$ (spacer)	5	Undoped	
$GaAs_{0.96}Bi_{0.04}$ (quantum well)	7	Undoped	370°C
$Al_{0.15}Ga_{0.85}As$ (spacer)	5	Undoped	580°C
$Al_{0.15}Ga_{0.85}As$ (barrier)	10	Si-1 $\times 10^{18}\mathrm{cm}^{-3}$	
GaAs buffer layer			
GaAs semi-insulating substrate			

Table II: Sample codes and annealing parameters.

Material	Code	Annealing Temperature (°C)	Annealing Time (s)
$Al_{0.15}Ga_{0.85}As/GaAs$	TNR00	as-grown (0)	-
$Al_{0.15}Ga_{0.85}As/GaAs_{0.96}Bi_{0.04}$	TNBi04	as-grown (0)	-
	TNBi04A	700	60
	TNBi04B	350	180

Results and Discussion

a) Experimental Results

Figure 1 shows magnetoresistance results for all samples taken at different applied electric fields at 4.2 K. The applied electric field is increased until the amplitude of SdH oscillations is damped. Pronounced SdH oscillations are observed at 4.2 K for all samples. The amplitude of the SdH oscillations increase monotonously with increasing magnetic field for the as-grown (TNBi04) and the GaAsBi sample annealed at 700°C (TNBi04A), while the increase is less monotonous for the reference sample (TNR00) and the GaAsBi sample annealed at 350°C (TNBi04B).

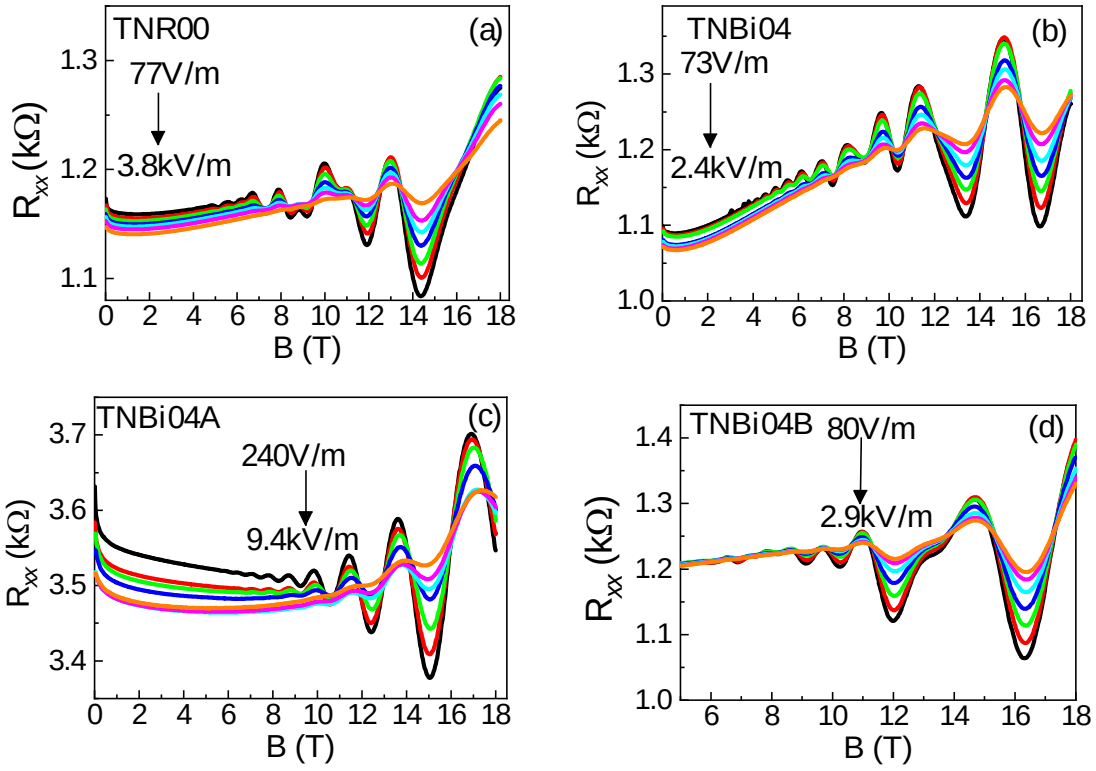

Figure 1: Magnetoresistance data taken with varying applied electric field at 4.2K. The applied electric field range is shown on the graph. The different line colors represent magnetoresistance curves taken at different applied electric field intensities.

The unstable characteristic of the SdH oscillations with the increasing magnetic field is an indication of the contribution from more than one oscillation frequency. A Fast Fourier Transformation (FFT) method was applied to the magnetoresistance data to determine the number of subband levels contributing to the conductivity of samples and period of the SdH oscillations. We obtain two oscillation frequencies for the samples TNR00 and TNBi04B as seen in Figure 2, resulting from two occupied electron subbands, and one for samples TNBi04 and TNBi04A. Even the sample structures are identical for Bi-containing samples, the observation of one or two occupied electron subbands are related to the different 2D electron density in the samples (see Table III) and the reason behind this observation is explained in detail in our previous paper [14]

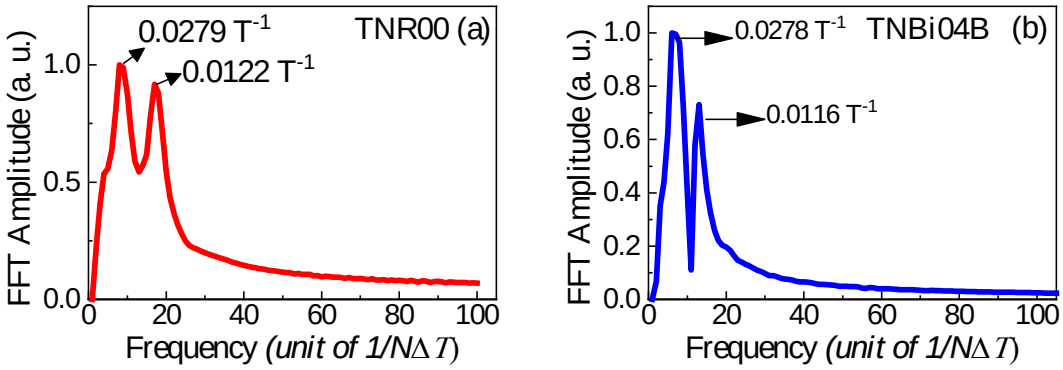

Figure 2: Fast Fourier Transform (FFT) of fitting of background removed results of a) TNBi00 and b) TNBi04B[14]

In order to exclude the effect of slow varying long-period background magnetoresistance and to separate the short-period SdH oscillations, the second derivative was taken. Figure 3 shows the second derivative of the SdH oscillations taken at different applied electric fields.

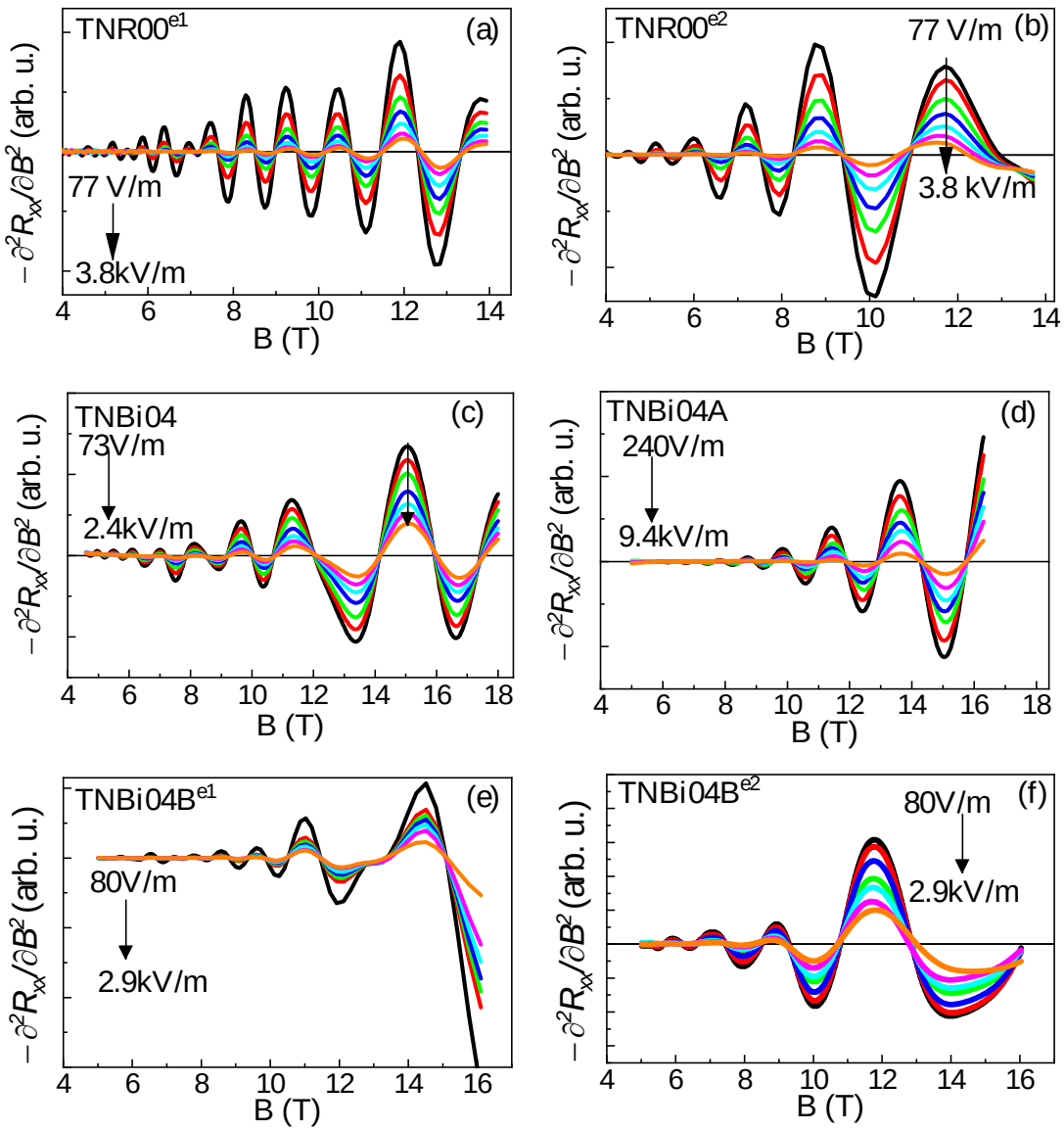

Figure 3: Second derivatives of the magnetoresistance data measured at 4.2K as a function applied electric field for all the samples. a-b and e-f represent the separated SdH oscillations of two subbands for the reference sample (TNR00) and the GaAsBi sample annealed sample at 350°C (TNBi04B), respectively. The applied electric field range is shown on the graph. The e1 and e2 superscripts correspond to the first and second subbands.

The temperature-dependent damping of the SdH oscillations at a fixed magnetic field is determined as a function of the temperature, magnetic field and the electron effective mass with an assumption of constant Dingle factor [16,21,22]

$$\frac{A(T_L)}{A(T_{L0})} = \frac{T_L sinh\left(\frac{2\pi^2 m_e^* k_B T_{L0}}{\hbar e B}\right)}{T_{L0} sinh\left(\frac{2\pi^2 m_e^* k_B T_L}{\hbar e B}\right)} \quad (1)$$

where m_e^* is the effective mass, A(T_L) and $A(T_{L0})$ are the amplitudes of the SdH oscillation peak observed at lattice temperatures T_L ($T_L > T_{L0}$) and T_{L0}, respectively. For III-V alloys, at temperatures below ≈40 K, the optical phonon population is negligibly small; therefore, acoustic phonon scattering is the only scattering mechanism for energy relaxation. There are two commonly used experimental methods to determine the electron temperature in the acoustic phonon regime [17]: i) if the material degenerates, a comparison of the electric field and lattice temperature-dependent SdH measurements can be used to determine the electron temperature, and ii) if the material does not degenerate, the electron temperature can be determined as a function of the applied electric field by comparing the electric field dependent and lattice temperature-dependent mobility curves. The samples used in this study are highly degenerate satisfying the $(E_F - E_1)/k_BT \gg 1$ condition [14], where E_F is Fermi level and E_1 is the first quantized electron energy level in QW. Therefore, we benefit from the electric field and lattice temperature-dependent amplitude variation of SdH oscillations to determine electron temperature.

The amplitude variation of the SdH oscillations with applied electric field is explained in terms of electric field-induced electron heating, therefore the lattice temperature, T_L, can be replaced by the electron temperature T_e in Eq. 1. T_e can be found by comparing the relative amplitudes of the SdH oscillations as functions of temperature and electric field *via*

$$\left[\frac{A(T_L)}{A(T_{L0})}\right]_{F=F_0} = \left[\frac{A(F)}{A(F_0)}\right]_{T_L=T_{L0}} \tag{2}$$

where F_0 and T_{L0} are the lowest applied electric field and the base temperature T_{L0} = 4.2 K, where experiments were carried out. The left side of *Eq*. 2 is related to the lattice temperature-dependent results; analysis of the SdH oscillations was presented in our previous paper [14]. Therefore, we do not discuss lattice temperature-dependent results here. The obtained parameters (2D carrier density, electron effective mass, Fermi level, transport mobility) from analysis of the temperature dependence of the magnitude of the SdH oscillations are shown in Table III.

Table III: The material parameters used in the scattering calculations. The parameters for GaAs are taken from *Refs*. [23,24] and the GaAsBi parameters are taken from *Refs*. [25–28]. The parameters determined from this study are designated as (Exp.). The second subband parameters for TNR00 and TNBi04B are given in parenthesis.

Parameters	Symbol	TNR00	TNBi04	TNBi04A	TNBi04B
Electron effective mass, *(Exp.)*[14]	m_e^* (m_e)	0.080 (0.073)	0.077	0.078	0.076 (0.066)
2D carrier density, *(Exp.)*[14]	$N_{2D}(10^{16}m^{-2})$	3.96 (1.76)	2.56	3.6	4.00 (1.73)
Hall carrier density, *(Exp.)*	$N_{2D}(10^{16}m^{-2})$	11.64	11.61	9.09	10.7
Transport mobility, *(Exp.)*[14]	μ_t(m^2/Vs)	0.22 (0.121)	0.185	0.068	0.066 (0.124)
Fermi Level, *(Exp.)*[14]	$(E_F - E_i)$ (meV)	121 (58)	80	111	127 (63)
Quantum well width	L (nm)	7			
Power Loss exponent	γ	3.1(2.9)	2.4	4.2	2.3 (2.3)
Power Ratio	P_{def}/P_{piezo}	8.3(2.1)	1.1	0.001	0.5 (0.2)
Critical Temperature	T_C (K)	35(24)	29	34	36 (24)
Deformation potential	Ξ (eV)	9.5 (7)	7.3	0.5	4 (4.2)
Crystal density[23,27]	ρ (10^3kg/m^3)	5.32	5.44		
Sound velocity[23,27]	v_S (10^3m/s)	4.79	4.75		
Electromechanical coupling constant[23,27]	K_{av}^2	0.025	0.045		
Dielectric constant[26,28]	ε (ε_0)	12.9	11.3		
Elastic constants[23,27]	C_{11} (10^{11}dyn/cm^2)	12.21	7.3		
Elastic constants[23,27]	C_{12} (10^{11}dyn/cm^2)	5.66	3.27		
Elastic constants[23,27]	C_{44} (10^{11}dyn/cm^2)	6	3.6		
Piezoelectric stress constant[24]	e_{14} (C/m^2)	-0.16	-0.16		

Figure 4 shows an illustration on how to define the electron temperature with a comparison of normalized amplitudes of the SdH oscillations at a fixed magnetic field as a function of the lattice temperature at the lowest applied electric field (F_0) and as a function of the applied electric field at 4.2 K (T_{L0}) for TNBi04. The normalized amplitudes are obtained from the last three SdH oscillations of the magnetotransport curves presented in Figure 3. The electric field dependence of the amplitude of SdH oscillations is calculated by using Eqs.1-2, by replacing T_L by T_e.

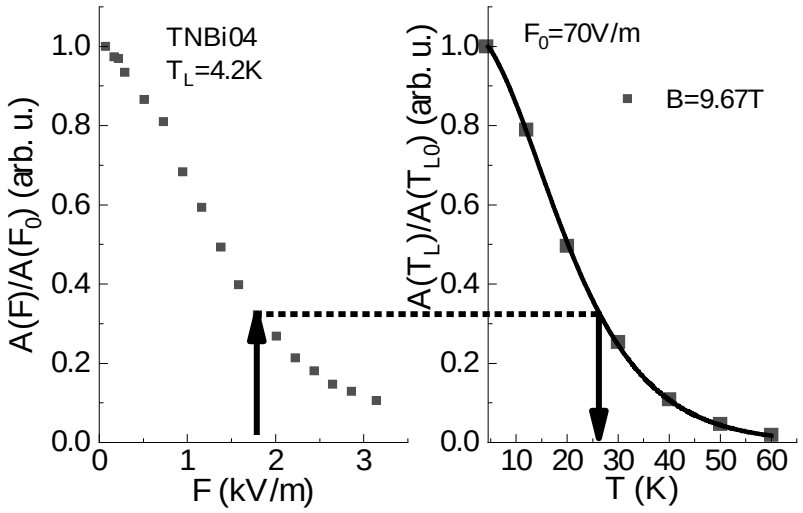

Figure 4: The amplitude ratio of the SdH oscillations as a function of applied electric field (left) and lattice temperature (right) at a fixed magnetic field of 9.67T for sample TNBi04. The electron temperature is obtained by comparing the lattice temperature and electric field dependencies of the normalized amplitudes of SdH oscillations. The squares represent experimental results, while the solid line in the right graph is calculated by using Eqs. 1-2, by replacing T_L by T_e.

Figure 5 shows the electron temperature *versus* applied electric field for all the samples at B ≈9.6 T. Measurements at different the magnetic fields show that the electron temperature is independent of magnetic field. It is obvious that incorporation of Bi in the GaAs lattice does not affect the electron temperature. However, variation is observed for the sample annealed at 700°C (TNBi04A). Furthermore, the electron temperature has an almost linear dependence on the applied electric field, which is an indication of the linear contribution of electron temperature to the power loss mechanism. The dependence tends to deviate from linear at higher electric fields for all the samples, as expected [29,30]. The lower electron temperature at the same applied electric field for TNBi04A can be related to a lower Hall carrier density (see Table III). It should be noted that the Hall carrier density is higher than the 2D carrier density for all the samples studied, indicating some carriers in the barrier layer. However, the SdH oscillations only give information about the transport characteristic of the 2D electron gas.

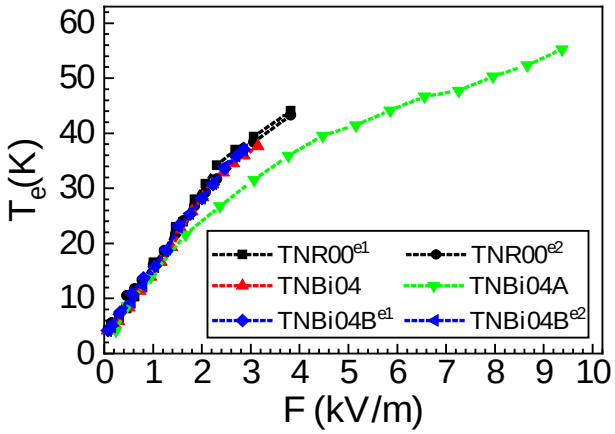

Figure 5: Electron temperature *versus* electric field for all samples at $B \approx 9.6$T. The electron temperature is obtained by comparing the lattice temperature and electric field dependencies of the amplitudes of SdH oscillations as depicted in Figure 3. The e1 and e2 superscripts correspond to the first and second subbands. The dotted-line is a guide to the eye.

b) Analyzing the power loss mechanisms of hot electrons in 2D

In the steady state, the power supplied from the applied electric field is equal to the power loss via the emission of acoustic phonons at low temperatures. The power loss per electron, P, can be calculated by

$$P = e\mu_t F^2 \tag{3}$$

where F is the applied electric field and μ_t is the quantum transport mobility. We have found that μ_t is almost independent of temperature and applied electric field between 4.2 and 60K. The effect of the Bi atoms on the quantum transport mobility is discussed in our previous study[14]. The experimentally determined values for electron mobility and effective electron mass are presented in Table III. The power loss *per* electron is calculated using *Eq*. 3 and plotted as a function of electron temperature in Figure 6.

The magnitude of the power loss *per* electron for the first subband of the Bi-free (TNR00) and as-grown Bi-containing samples (TNBi04) is almost the same. After annealing at 350°C, the magnitude of the power loss decreases. Since the only difference which can affect the power loss is 2D electron density (see Table III), the observed change in power loss per electron versus electron temperature can be related to the 2D electron density. In the following, the characteristic and variation of the power loss against electron temperature curves in Figure 6 will be explained in detail by fitting analytical expressions to the experimental data.

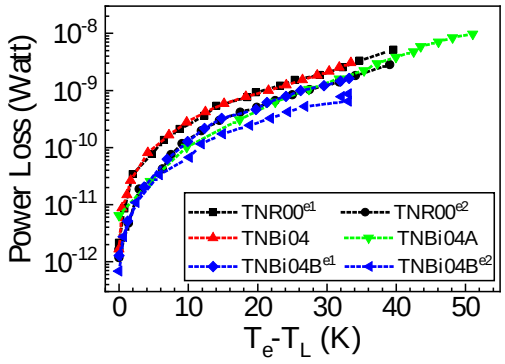

Figure 6: Power loss *per* electron *versus* electron-temperature for all the samples at B ≈ 9.6T. Power loss is calculated using Eq. 3. The e1 and e2 superscripts correspond to the first and second subbands. The dotted-lines are a guide to the eye.

Analysis of the power loss mechanism due to acoustic phonon scattering has been carried out in the low- and high-temperature regimes in previous reports [15–18,29–32]. At the low-temperature regime (Bloch-Grüneisen regime), the phonon population diminishes and the Pauli exclusion principle determines the allowed scattering process. At the high-temperature regime (equipartition regime), the phonon distribution can be considered as $n(\omega_q) \approx k_B T/\hbar\omega_q$, where $\hbar\omega_q$ is the acoustic-phonon energy at wavevector q. In very low temperatures, only small-angle scattering is allowed.

For our samples, the reduced Fermi level satisfies the $(E_F - E_{1,2}) \gg k_B T_L$ condition and therefore the power loss mechanism is expected to have degenerate behavior [15,29,30]. In this case, the power loss dependencies on electron temperature for the unscreened deformation potential (non-polar) and the unscreened piezoelectric (polar) scattering are $P_{np}^{LT}\ \alpha\ (T_e^5 - T_L^5)$ and $P_p^{LT}\ \alpha\ (T_e^3 - T_L^3)$ in a very low-temperature regime, respectively. In the low-temperature regime for a degenerate 2D electron gas, where the electron temperature satisfies $T_e \ll T_e^c\ (= [\,8m_e^* V_S^2 (E_F - E_{1,2})]^{\frac{1}{2}}/k_B)$, the power loss is given by the linear combination of these two scattering mechanisms as [15,29,30]

$$P = C_{np}\,[(k_B T_e)^5 - (k_B T_L)^5] + C_p\,[(k_B T_e)^3 - (k_B T_L)^3] \tag{4}$$

where

$$C_{np} = \frac{6\Xi^2 {m_e^*}^2 L}{\pi^3 \rho \hbar^7 v_S^4 N_{2D}} \tag{5a}$$

and

$$C_p = \frac{e^2 K_{av}^2 m_e^{*2}}{2\pi^2 \varepsilon \hbar^5 k_F N_{2D}} \tag{5b}$$

which are the magnitudes of the deformation potential and piezoelectric interaction, respectively. Ξ is the acoustic deformation potential energy, L is the quantum well width, ρ is the crystal mass density, v_S is the speed of sound, N_{2D} is the 2D electron density, K_{av} is the average electro-mechanical coupling constant, ε is the static dielectric constant, and $k_F\left(=\sqrt{2\pi N_{2D}}\right)$ is the 2D Fermi wavevector.

In the high-temperature regime for a degenerate 2D electron gas, where the electron temperature satisfies $T_e \gg T_e^c$, the power loss can be given by [15,29,30]

$$P = (\tilde{C}_{np} + \tilde{C}_p)(k_B T_e - k_B T_L) \tag{6}$$

where,

$$\tilde{C}_{np} = \frac{3\Xi^2 m_e^{*2}}{2\rho\hbar^3 L} \tag{7a}$$

and

$$\tilde{C}_p = \frac{3e^2 K_{av}^2 m_e^{*2} V_S^2}{4\pi\varepsilon\hbar^3 L N_{2D}} \tag{7b}$$

which are the magnitudes of the deformation potential and piezoelectric interaction for the high-temperature regime, respectively. Finally, the power loss in the intermediate regime between the low- and high-temperature regimes can be obtained as a weighting of both contributions [15,29,30],

$$P = f(T_e, T_L)\left(\tilde{C}_{np} + \tilde{C}_p\right)(k_B T_e - k_B T_L) \tag{8}$$

where, $\tilde{C}_{np}$ and $\tilde{C}_n$ are given in *Eqs*. 7a and 7b, respectively, and

$$f(T_e, T_L) = \frac{sinh(x_L - x_e)}{sinh\, x_L\, sinh\, x_e}\left[\frac{x_L x_e}{x_L - X_e}\right] \tag{9}$$

where, $x_e = \frac{\hbar\omega}{2k_B T_e}$, $x_L = \frac{\hbar\omega}{2k_B T_L}$, and $\hbar\omega\ (= \sqrt{2}\ \hbar v_S k_F)$ is the acoustic-phonon energy. The first pre-factor of *Eq.* 8 approaches unity at high temperatures and decreases exponentially at low temperatures; thereby making this relation a useful approximation for the intermediate regime.

The power loss *per* electron dependence on electron temperature has been often approximated by the relationship [15,16]

$$P = A\left(T_e^{\gamma} - T_{L0}^{\gamma}\right) \tag{10}$$

where T_{L0} is the lowest lattice temperature and A is a proportionality constant, which depends on 2D carrier density, elastic constants, effective mass, speed of sound, QW thickness, and coupling constants. The value of the exponent γ, which is obtained by fitting Eq. 10 to the experimental data, gives information about the temperature range of energy loss of 2D electrons as well as simplified information about the energy loss regimes and mechanisms [19,30].

The γ parameter for each populated subband is found to be between 2.1 and 4.2 by fitting Eq. 10 to the experimental data (see Table III). This can be explained by considering that the energy relaxation of hot phonons is due to acoustic phonons *via* the mixed contribution of unscreened piezoelectric and deformation potential scattering. The screening effect is expected to increase for a 2D electron gas as the temperature decreases [33,34]. Since the γ parameter is smaller than 5 for all samples, the 2D carrier density is high enough such that, at 4.2K, the electron-acoustic phonon interaction is not screened by 2D electrons. Barlow *et al.* [35] found the γ value between 3 and 5 in $In_{0.53}Ga_{0.47}As$/InP QW structures and they concluded that the power loss is achieved by both unscreened piezoelectric and deformation potential interactions. The value of $\gamma \cong 3$ is also typical for experiments that are carried out between the low- and high-temperature ranges, *i.e*, the intermediate temperature regime [16,18,35]. In light of these reports, it can be concluded that the power loss mechanisms occur in intermediate-temperature regime and the interactions are unscreened by 2D electrons for the samples studied.

To determine the power loss in the acoustic phonon regime, magnetoresistance experiments are usually carried out in the temperature range between 2 and 20 K, which is between the low- and high-temperature regimes. Therefore, we have carried out the measurements at 4.2 K, which indeed corresponds to the intermediate-temperature regime. We have also found γ to have values between 2.1 and 4.3, therefore, it is more suitable to use *Eq*. 8 to investigate the electron temperature dependence on the power loss rate of the 2D electron gas. However, to verify that the most suitable regime for our results is the intermediate temperature regime, we have fitted the experimental $P(T_e)$ data with the low (*Eq.* 4), high (*Eq.* 6), and intermediate (*Eq.* 8) temperature regime expressions. In all cases, we have taken the deformation potential energy as a fit parameter. Figure 7 shows each fit for sample TNBi04, where we find the intermediate-temperature regime fitting function (*Eq.* 8) gives the best fit to the experimental data.

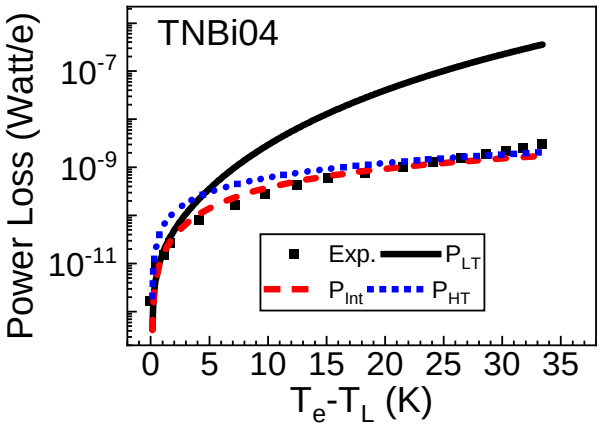

Figure 7: Electron temperature dependence of the power loss rate for TNBi04. Black square symbols represent experimental results. Solid, short-dashed, and short-dotted lines are ascribed for low (LT), intermediate (Int.), and high (HT) temperature regimes, respectively.

By doing the same fitting process for all sample data, we found that Eq. 8 consistently gave the best fit results. Therefore, we only present the analysis of the results using the intermediate temperature regime of the power loss mechanism defined by Eq. 8. In the calculations, most of the physical parameters of GaAsBi were determined from Vegard's law using parameters of the binary endmembers of GaAs and GaBi. Specifically, Wang and Ye [27] calculated the elastic constants of the GaBi semimetal using the first-principle plane-wave pseudopotential method; therefore, we exploit their results in our study. One should pay attention to *Eqs*. 5 and 7, because there are two unknown parameters: deformation potential energy and piezoelectric constant for the GaAsBi material. Batool *et al.* [36] reported that the deformation potential energy of Bi-containing alloys is drastically affected by introduction of Bi atoms into GaAs. To the best of our knowledge, there are no studies on the piezoelectric properties of GaBi or Bi-containing alloys. However, in conventional III-V alloys the alloying process does not significantly change the piezoelectric constant, in contrast with the deformation potential; therefore, we used the piezoelectric stress constant for GaAs, while the deformation potential energy was left as an adjustable parameter for Bi-containing samples [24,37]. All parameter values used for the calculations are given in Table III.

Figure 8 shows the experimental data with fits for all samples. The Bi-containing samples exhibit an identical structure with each other; the observed variations in the magnitude of power loss can be related to disparities among 2D electron density, electron mobility and the number of occupied subbands (see the parameters in Table III).

The best fit to the experimental data is obtained with deformation potential energy as 9.5eV (e1) and 7.0eV (e2) for the Bi-free sample (TNR00), which is close to the known value for single subband population in GaAs [17,24,38]. Although the power exponent of γ= 3.1 indicates that the power loss mechanism can include both polar (piezoelectric) and non-polar (deformation) scattering in the intermediate temperature range, the deformation potential dominates over piezoelectric scattering with a ratio of P_{def}/P_{piezo} = 8.3 for the first subband, where the best fit is obtained at electron temperatures lower than 30K. However, the ratio for the second subband given in Table III is lower than for the first subband, which may be an effect of lower electron density of the second subband.

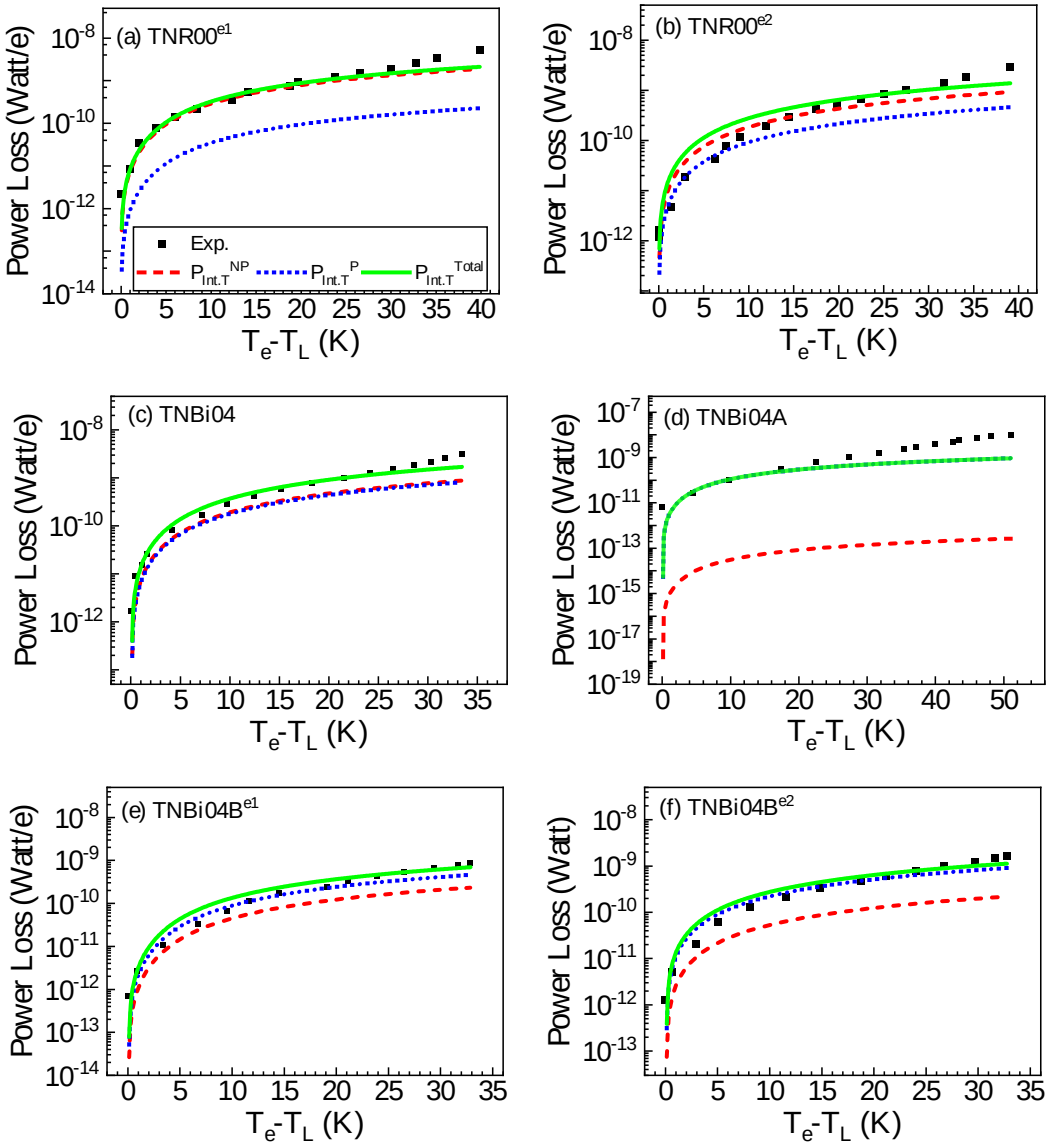

Figure 8: Power loss rate as a function of electron temperature for all the samples. Black square symbol represents experimental results. The dashed, dotted, and solid lines are ascribed for deformation (non-polar, NP), piezoelectric (polar, P) and total power loss results

It is worth noting that all the power loss equations given above are derived for the single subband occupation. However, the second quantized energy level in TNR00 and TNBi04B is occupied by electrons because the carrier density in TNR00 and TNBi04B is greater than that in TNBi04 and TNBi04A [14]. The total theoretical analysis of the energy loss per carriers for two-subband occupation is described as $P_{total} = P_{11} + P_{12} + P_{21} + P_{22}$, where P_{ii} is the energy loss for electrons in *i*th subband and P_{ij} refers to the interaction of the electron at the *i*th subband with the *j*th subband level [16,39]. The expressions derived for the electron temperature dependencies of the intersubband scattering processes P_{12} and P_{21} are complex and different from the single band occupation characteristic of P_{11} and P_{22}. Even as the 2D carrier concentration in the second subband given in Table III is smaller than that in the first subband for all the samples having two subbands, E_F lies above the second subband and the separation of the E_2 and E_1 is high enough to weaken the interaction between the E_1 and E_2 levels. Therefore, P_{12} and P_{21} can be ignored [16,40]. The total power loss can be approximated as $P = P_{11} + P_{22}$ and the Eqs. 3-9 can be used separately for the scatterings in the first subband (P_{11}) and in the second subband (P_{22}).

Decrease of the deformation potential energy (7.0eV) and the contribution of the deformation potential scattering to the power loss for the second subband of TNR00 can be related to the smaller 2D electron density of the second subband. The deformation potential (*Eq.* 7a) is independent of the carrier concentration, while piezoelectric scattering (*Eq.* 7b) is inversely proportional to carrier concentration. The decrease of carrier concentration in the second subband increases the contribution of piezoelectric scattering to the total power loss. Therefore, the deformation potential energy of 7.0 eV for the second subband can originate from the smaller carrier concentration in the second subband.

Incorporation of Bi into GaAs slightly changes the magnitude of the power loss parameters for TNBi04 and TNBi04B, but the difference is significant for TNBi04A. As seen in Figure 8c, the power dissipation for the a-grown Bi-containing sample (TNBi04) is determined as a mix of the deformation potential and piezoelectric scattering as the power ratio P_{def}/P_{piezo} is 1.1. Moreover, the deformation potential is almost the same as the second subband of the Bi-free sample (TNR00). Comparison of the deformation potential

energy for TNBi04 with that of the first subband of TNR00 shows that it becomes smaller after introducing Bi atoms into GaAs. In our previous studies, we experimentally showed that the temperature dependence of the bandgap weaken after introducing Bi into GaAs[20,41,42]. Temperature dependence of the bandgap is proportional to the thermal expansion coefficient of the material, which becomes smaller as a result of the incorporation of Bi [20,42,43]. It is known that the deformation potential of the electronic states at the Brillouin zone centre of the semiconductor fundamentally affects the transport properties of the carriers. The deformation potential of the semiconductor depends on the elastic constants C_{11} and C_{12} [24]. The radius of the Bi atom is larger than the As atom, therefore introducing Bi into GaAs reduces the elastic constant of the GaAsBi alloy. Furthermore, Bi containing alloys contain various types of defects, which also affect the elastic constant. Therefore, a smaller value of the deformation potential for TNBi04 can be expected.

None of the analytical expressions gives a gratifying fit to the experimental data for TNBi0A and the deformation potential energy is determined as 0.5eV, which is not realistic and thus will not be discussed further. We have shown in our previous paper [14] that the high-temperature thermal annealing deteriorates the electrical properties of this sample. In addition, PL intensity of the sample decreases with thermal annealing at 700 ºC, which is also an indication of degradation of the crystal quality of the sample, therefore it is not meaningful to discuss the reason of the determined unrealistic value for the deformation potential in this sample.

It is observed that PL intensity increases after thermal annealing at 350 ºC. This results showed that thermal annealing under specific conditions could remove some defects in GaAsBi samples and subsequently enhance electrical and optical properties, which could explain the lower deformation potential energy of 4.0eV for e1 and 4.2eV for e2 in TNBi04B. Also, it is clear from Figure 8 c, e, and f that the power loss mechanism in TNBi04B switches from deformation potential to piezoelectric scattering.

The energy relaxation time for each subband can be obtained from the power loss measurements *via*

$$P = \frac{\langle \hbar\omega \rangle}{\tau_E} \frac{(k_B T_e - k_B T_L)}{k_B T_e} \tag{10}$$

where $\langle \hbar\omega \rangle$ is $\sqrt{2}\hbar v_s k_F$. Figure 9 shows the energy relaxation time as a function of T_e-T_{L0}, which indicates that the relaxation times are almost the same for all samples.

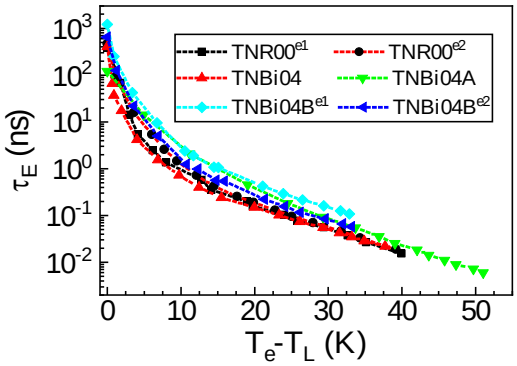

Figure 9: Energy relaxation time versus T_e-T_L for all the samples.

As seen in Figure 9, the trend of energy relaxation time *versus* electron temperature is similar at whole electron temperatures, but its magnitude is slightly different from sample to sample, which can be related to the different electron mobilities and 2D carrier densities. The large values of τ_e at low electron temperatures at around 4.2K (T_e-T_L = 0K) for all samples studied that indicate that the relaxation time is not sufficiently efficient for cooling of the device *via* acoustic phonon scatterings; thus a fast increase of the electron temperature is observed when the input power is increased (Fig. 6). An observed fast droop at the energy relaxation time as electron temperatures increases to 9K (T_e-T_L = 5K) with an order of three (from 1μs to 1ns) means that the samples are effectively cooled *via* acoustic phonon scatterings. The values of τ_e are higher with almost one order at 4.2K (T_e-T_L = 0K) than the one reported for InGaAs/InAlAs [16], but similar to the ones observed in GaInNAs/GaAs [16,19].The lower electron mobility in GaAsBi and its counterpart GaInNAs makes energy relaxation times larger than that in QW structures based on conventional III-V alloys such as InGaAs and GaAlAs. However, as electron temperature slightly increases, energy relaxation time becomes smaller in our samples than that in n-type modulation GaInNAs/GaAs QWs [16,19]. Since the localized Bi level does not significantly affect the CB, effective electron mass in GaAsBi is smaller compared to the effective mass of electrons in GaInNAs, which enable efficient cooling of hot electron in GaAsBi/GaAs QW structures above 9K. It can be concluded that under high electric field regime a device based on GaAsBi is more beneficial than a device based on GaInNAs thanks to its more efficient cooling process *via* acoustic phonon scatterings.

Conclusion

The power loss mechanisms of 2D electrons in n-type modulation doped AlGaAs/GaAsBi QW have been investigated by analyzing the variation of the amplitudes of SdH oscillations as a function of the applied electric field at 4.2K. The energy relaxation of 2D electrons is found to be in the intermediate-temperature range, by comparing experimental results with the theoretical power loss models of a 2D electron gas. In the intermediate-temperature range, the deformation component is dominant over the piezoelectric component of the acoustic phonon emission for Bi-free samples. The incorporation of Bi decreases the electron temperature and alters the power loss mechanism from one dominated by deformation potential to one with equal contribution of deformation and piezoelectric scattering. After thermal annealing at 350°C, the power loss amplitude and deformation potential energy are decreased, and the power loss mechanism switches to a dominant piezoelectric scattering mechanism. The electron relaxation times are determined as a function of electron temperature and are found to be almost the same with Bi-free, Bi-containing as-grown and annealed samples with a negligible difference at the amplitude of energy relaxation times, which can be arisen from differences in electron mobility and 2D electron carrier density.

Acknowledgements

This work is supported by The Scientific and Technical Research Council of Turkey (TUBITAK) under Grant No. 115F517.

References

[1] Francoeur S, Seong M-J, Mascarenhas A, Tixier S, Adamcyk M and Tiedje T 2003 Band gap of GaAs1−xBix, 0<x<3.6% *Appl. Phys. Lett.* **82** 3874–6

[2] Bahrami-Yekta V, Tiedje T and Masnadi-Shirazi M 2015 MBE growth optimization for GaAs 1− x Bi x and dependence of photoluminescence on growth temperature *Semicond. Sci. Technol.* **30** 094007

[3] Kudrawiec R, Kopaczek J, Polak M P, Scharoch P, Gladysiewicz M, Misiewicz J, Richards R D, Bastiman F and David J P R 2014 Experimental and theoretical studies of band gap alignment in GaAs 1−x Bi x /GaAs quantum wells *J. Appl. Phys.* **116** 233508

[4] Kopaczek J, Linhart W M, Baranowski M, Richards R D, Bastiman F, David J P R and Kudrawiec R 2015 Optical properties of GaAsBi/GaAs quantum wells: Photoreflectance, photoluminescence and time-resolved photoluminescence study *Semicond. Sci. Technol.* **30** 94005

[5] Ludewig P, Knaub N, Hossain N, Reinhard S, Nattermann L, Marko I P, Jin S R, Hild K, Chatterjee S, Stolz

W, Sweeney S J and Volz K 2013 Electrical injection Ga(AsBi)/(AlGa)As single quantum well laser *Appl. Phys. Lett.* **102** 242115

[6] Marko I P, Ludewig P, Bushell Z L, Jin S R, Hild K, Batool Z, Reinhard S, Nattermann L, Stolz W, Volz K and Sweeney S J 2014 Physical properties and optimization of GaBiAs/(Al)GaAs based near-infrared laser diodes grown by MOVPE with up to 4.4% Bi *J. Phys. D. Appl. Phys.* **47** 345103

[7] Fluegel B, Francoeur S, Mascarenhas A, Tixier S, Young E C and Tiedje T 2006 Giant spin-orbit bowing in GaAs1-xBix *Phys. Rev. Lett.* **97** 11–4

[8] Pursley B, Luengo-Kovac M, Vardar G, Goldman R S and Sih V 2013 Spin lifetime measurements in GaAsBi thin films *Appl. Phys. Lett.* **102**

[9] Kado K, Fuyuki T, Yamada K, Oe K and Yoshimoto M 2012 High hole mobility in GaAs 1-xBi x alloys *Jpn. J. Appl. Phys.* **51** 8–11

[10] Cooke D G, Hegmann F A, Young E C and Tiedje T 2006 Electron mobility in dilute GaAs bismide and nitride alloys measured by time-resolved terahertz spectroscopy *Appl. Phys. Lett.* **89** 122103

[11] Beaton D A, Lewis R B, Masnadi-Shirazi M and Tiedjep T 2010 Temperature dependence of hole mobility in GaAs1−xBix alloys *J. Appl. Phys.* **108** 083708

[12] Kini R N, Bhusal L, Ptak A J, France R and Mascarenhas A 2009 Electron hall mobility in GaAsBi *J. Appl. Phys.* **106**

[13] Fluegel B, Kini R N, Ptak a. J, Beaton D, Alberi K and Mascarenhas A 2011 Shubnikov-de Haas measurement of electron effective mass in GaAs 1− x Bi x *Appl. Phys. Lett.* **99** 162108

[14] Donmez O, Aydın M, Ardalı Ş, Yıldırım S, Tıraş E, Nutku F, Çetinkaya Ç, Çokduygulular E, Puustinen J, Hilska J, Guina M and Erol A 2020 Electronic transport in n-type modulation-doped AlGaAs/GaAsBi quantum well structures: influence of Bi and thermal annealing on electron effective mass and electron mobility *Semicond. Sci. Technol.* **35** 025009

[15] Balkan N 2012 Hot Electron Energy and Momentum Relaxation *Semiconductor Research: Experimental Techniques* Springer Series in Materials Science vol 150, ed A Patane and N Balkan (Berlin: Springer) pp 63–92

[16] Tiras E, Cankurtaran M, Çelik H and Balkan N 2001 Hot electron energy relaxation via acoustic phonon emission in modulation-doped In0.53Ga0.47As/In0.52Al0.48As heterojunctions with double-subband occupancy *Phys. Rev. B* **64** 085301

[17] Balkan N, Çelik H, Vickers A J and Cankurtaran M 1995 Warm-electron power loss in GaAs/Ga1-xAlxAs multiple quantum wells: Well-width dependence *Phys. Rev. B* **52** 17210–22

[18] Cankurtaran M, **?**elik H and Balkan N 2002 Electron Energy Relaxation via Acoustic Phonon Emission in GaAs/Ga1?xAlxAs Multiple Quantum Wells: Effects of Base Lattice Temperature *Phys. status solidi* **229** 1191–204

[19] Tiras E and Ardali S 2013 Electron and hole energy relaxation rates in GaInNAs/GaAs quantum wells via deformation potential and piezoelectric scattering *Phys. Status Solidi Basic Res.* **250** 134–46

[20] Cetinkaya C, Cokduygulular E, Nutku F, Donmez O, Puustinen J, Hilska J, Erol A and Guina M 2018 Optical properties of n- and p-type modulation doped GaAsBi/AlGaAs quantum well structures *J. Alloys Compd.* **739** 987–96

[21] Coleridge P T 1990 Inter-subband scattering in a 2D electron gas *Semicond. Sci. Technol.* **5** 961–6

[22] Dönmez Ö, Sarcan F, Erol A, Gunes M, Arikan M, Puustinen J and Guina M 2014 Magnetotransport study on as-grown and annealed n- and p-type modulation-doped GaInNAs/GaAs strained quantum well structures *Nanoscale Res. Lett.* **9** 141

[23] Vurgaftman I, Meyer J R and Ram-Mohan L R 2001 Band parameters for III–V compound semiconductors and their alloys *J. Appl. Phys.* **89** 5815–75

[24] Adachi S 1985 GaAs, AlAs, and Al x Ga 1− x As: Material parameters for use in research and device applications *J. Appl. Phys.* **58** R1–29

[25] Ben Sedrine N, Moussa I, Fitouri H, Rebey A, El Jani B and Chtourou R 2009 Spectroscopic ellipsometry study of GaAs1−xBix material grown on GaAs substrate by atmospheric pressure metal-organic vapor-phase epitaxy *Appl. Phys. Lett.* **95** 011910

[26] Ulutas K, Yakut S, Bozoglu D, Deger D, Arslan M and Erol A 2019 Influence of Bi on dielectric properties of GaAs1−xBix alloys *Mater. Sci.* **37** 244–8

[27] Wang S Q and Ye H Q 2003 First-principles study on elastic properties and phase stability of III–V compounds *Phys. status solidi* **240** 45–54

[28] Tumėnas S, Karpus V, Bertulis K and Arwin H 2012 Dielectric function and refractive index of GaBix As1-x (x = 0.035, 0.052, 0.075) *Phys. status solidi* **9** 1633–5

[29] Ridley B K 1996 The Electron Distribution Function *Electrons and Phonons in Semiconductor Multilayers* (Cambridge: Cambridge University Press) pp 275–310

[30] Ridley B K 1991 Hot electrons in low-dimensional structures *Reports Prog. Phys.* **54** 169–256

[31] Tiras E, Celik O, Mutlu S, Ardali S, Lisesivdin S B and Ozbay E 2012 Temperature dependent energy relaxation time in AlGaN/AlN/GaN heterostructures *Superlattices Microstruct.* **51** 733–44

[32] Tiras E, Ardali S, Arslan E and Ozbay E 2012 Energy relaxation rates in AlInN/AlN/GaN heterostructures *J. Electron. Mater.* **41** 2350–61

[33] Price P J 1982 Hot electrons in a GaAs heterolayer at low temperature *J. Appl. Phys.* **53** 6863–6

[34] Bennett C, Balkan N, Tanatar B, Celik H and Cankurtaran M 1998 The static and dynamic screening of power loss of a two-dimensional electron gas *Superlattices Microstruct.* **24** 25–32

[35] Barlow M J, Ridley B K, Kane M J and Bass S J 1988 Hot electron energy relaxation via acoustic phonon emission in InP/In0.53Ga0.47As heterostructures and single quantum wells *Solid. State. Electron.* **31** 501–

[36] Batool Z, Hild K, Hosea T J C, Lu X, Tiedje T and Sweeney S J 2012 The electronic band structure of GaBiAs/GaAs layers: Influence of strain and band anti-crossing *J. Appl. Phys.* **111** 113108

[37] Adachi S 1992 *Physical Properties of III-V Semiconductor Compounds: InP, InAs, GaAs, GaP, InGaAs, and InGaAsP* (USA: John Wiley & Sons)

[38] Hirakawa K and Sakaki H 1986 Energy relaxation of two-dimensional electrons and the deformation potential constant in selectively doped AlGaAs/GaAs heterojunctions *Appl. Phys. Lett.* **49** 889–91

[39] Straw A, Vickers A J and Roberts J S 1989 Energy relaxation in GaInAs/AlInAs heterojunctions and GaAs/AlGaAs multiple quantum wells *Solid. State. Electron.* **32** 1539–43

[40] Kreshckhuk M A, Martisov M Y, Polyanskaya T A, Savel'ev I G, Saidashev I I, Shik A Y and Sharmartsev Y V 1988 Role of higher subbands in relaxation of the energy of two-dimensional electron gas *Sov. Phys.-Semicond.* **22** 377

[41] Donmez O, Erol A, Arikan M C, Makhloufi H, Arnoult A and Fontaine C 2015 Optical properties of GaBiAs single quantum well structures grown by MBE *Semicond. Sci. Technol.* **30** 094016

[42] Sarcan F, Dönmez Ö, Kara K, Erol A, Akalın E, Çetin Arıkan M, Makhloufi H, Arnoult A and Fontaine C 2014 Bismuth-induced effects on optical, lattice vibrational, and structural properties of bulk GaAsBi alloys *Nanoscale Res. Lett.* **9** 119

[43] Gunes M, Ukelge M O, Donmez O, Erol A, Gumus C, Alghamdi H, Galeti H V A, Henini M, Schmidbauer M, Hilska J, Puustinen J and Guina M 2018 Optical properties of GaAs 1−x Bi x /GaAs quantum well structures grown by molecular beam epitaxy on (100) and (311)B GaAs substrates *Semicond. Sci. Technol.* **33** 124015